Near-threshold measurement of integrated Stokes parameters for Kr excited by polarized electrons

B. G. Birdsey, H. M. Al-Khateeb, M. E. Johnston,* T. C. Bowen,† and T. J. Gay
Behlen Laboratory of Physics, University of Nebraska, Lincoln, Nebraska 68588-0111

V. Zeman
Mathematics Department, University of Nottingham, Nottingham NG7 2RD, United Kingdom

K. Bartschat
Physics Department, Drake University, Des Moines, Iowa 50311

(Received 18 September 1998; revised manuscript received 12 March 1999)

We have made high-accuracy measurements of the integrated Stokes parameters for resonance fluorescence from polarized electron-impact excitation of the $4p^5 5p[5/2]\ ^3D_3$ and $4p^5 5p[5/2]^3D_2$ states of Kr. We report measurements in the region within 0.6 eV of threshold, which is below the first cascade threshold. We also present theoretical calculations of these Stokes parameters using a recently developed relativistic Breit-Pauli *R*-matrix code. In well *LS*-coupled systems, nonzero values of the integrated Stokes parameter P_2 signal relativistic effects (like continuum spin-orbit coupling, i.e., Mott scattering). A single value of $P_2 = 4(4) \times 10^{-3}$ at 12.0 eV was previously reported in this energy range [Furst *et al.*, Phys. Rev. A **47**, 3775 (1993)]. We have now measured P_2 at six different energies in this region to comparable precision. These results are consistent with $P_2 = 0$ and with the theory. We discuss the effect of the electron-beam energy width on the accuracy of the measurements. Even when such effects are accounted for, serious discrepancies remain between theoretical and experimental results for excitation of the intermediately coupled $^3D_2$ state. [S1050-2947(99)07907-X]

PACS number(s): 34.80.Dp

I. INTRODUCTION

With the advent of convergent-close-coupling (CCC) calculations [1,2], electron scattering amplitudes can be calculated very accurately over a broad energy range for H and He targets, as well as the light alkali-metal atoms. However, calculations involving heavy targets are hampered by the necessary inclusion of a larger number of target electrons as well as relativistic effects such as internal spin-orbit coupling and spin-orbit coupling to the continuum electron. Some progress has been made by using the Breit-Pauli *R*-matrix technique [3–5], particularly for impact excitation of heavy noble gases (HNGs). In this method, relativistic effects are accounted for perturbatively through the one-electron terms of the Breit-Pauli Hamiltonian [6].

We have been particularly interested in the relative Stokes parameter P_2 in angle-integrated transversely polarized electron-impact experiments. Under these conditions, observing a nonzero value of P_2 provides a clean test of relativistic effects, involving either atomic fine-structure or spin-orbit coupling to the continuum electron. If the spin and orbital angular momentum of the excited state are decoupled, only spin-orbit coupling of the free electron to the atom will produce nonzero values of P_2 [7–9]. Several years ago, we made a number of attempts to measure nonzero P_2 values in the HNGs Ne, Ar, Kr, and especially Xe, where the angle-integrated Mott scattering asymmetry should be largest. The statistical precision of those measurements was hampered by low-density targets which produce low count rates. Moreover, the theoretical calculations at that time predicted immeasurably small values of P_2 [8–10]. Since our initial work, other groups have also made measurements of integrated Stokes parameters in the HNGs, using incident polarized electrons [5,11–16].

More recently, several theoretical groups have investigated polarized electron-impact excitation of HNGs [5,17,18]. Of these theories, the *R*-matrix calculations clearly have the best chance of correctly predicting results within 1 eV of the excitation threshold. Interestingly, *R*-matrix calculations of Zeman *et al.* [5] predict values of P_2 as large as 6% near the excitation threshold of the well *LS*-coupled states $4p^5 5p[5/2]\,^3D_3$ in Kr and $5p^5 6p[5/2]\ ^3D_3$ in Xe. This provided us with the motivation to make additional high-precision measurements of P_2 in Kr, where the gap between the excitation threshold of the $^3D_3$ state and the excitation of the next higher state which can decay into the $^3D_3$ state is 0.7 eV. While the predicted values of P_2 are higher for Xe, the corresponding gap is only 0.3 eV, indicating that the count rates would be very low in the region where our measurements are free of contamination from cascades [19].

The Stokes parameters P_1, P_2, and P_3 are closely related to the detailed structure of the excited-state charge cloud. Generally, atomic excitation processes create anisotropic charge clouds whose detailed shape and angular momentum coupling are completely characterized by state multipoles. The angular distribution and polarization of the dipole emis-

*Present address: Department of Physics, University of Saint Thomas, 2115 Summit Ave., St. Paul, MN 55105-1096.

†Present address: HY-Tech Research Corporation, 104 Centre Court, Radford, VA 24141.

sion from these excited states carries information about the monopole, dipole, and quadrupole moments of the charge cloud [20]. However, the number of nonzero multipole moments depends on the collision symmetries in the experimental apparatus [21]. In the present experiment we excited the Kr target with a transversely polarized electron beam, but did not detect the scattered electrons in coincidence with the emitted photons (we made an ''angle-integrated'' measurement). Because of this planar symmetry, the number of possible independent multipole moments is reduced from eight to four integrated multipole moments: $\langle \mathcal{T}^{\dagger}_{00} \rangle$, $\langle \mathcal{T}^{\dagger}_{20} \rangle$, $\langle \mathcal{T}^{\dagger}_{11} \rangle$, and $\langle \mathcal{T}^{\dagger}_{21} \rangle$.

When viewing the excited-state fluorescence along the direction of the transverse electron polarization, the relative integrated Stokes parameters of the dipole radiation can be expressed as follows:

$$P_1 = \frac{I(0)-I(90)}{I(0)+I(90)} = \frac{\begin{Bmatrix} 1 & 1 & 2 \\ J & J & J_f \end{Bmatrix} \sqrt{\tfrac{3}{2}} \langle t^{\dagger}_{20} \rangle}{\dfrac{2(-1)^{J+J_f}}{3\sqrt{2J+1}} + \sqrt{\tfrac{1}{6}} G^I_2 \begin{Bmatrix} 1 & 1 & 2 \\ J & J & J_f \end{Bmatrix} \langle t^{\dagger}_{20} \rangle}, \tag{1}$$

$$P_2 = \frac{I(45)-I(135)}{I(45)+I(135)} = \frac{-\begin{Bmatrix} 1 & 1 & 2 \\ J & J & J_f \end{Bmatrix} \sqrt{\tfrac{3}{2}} \mathrm{Re} \langle t^{\dagger}_{21} \rangle}{\dfrac{2(-1)^{J+J_f}}{3\sqrt{2J+1}} + \sqrt{\tfrac{1}{6}} G^I_2 \begin{Bmatrix} 1 & 1 & 2 \\ J & J & J_f \end{Bmatrix} \langle t^{\dagger}_{20} \rangle}, \tag{2}$$

and

$$P_3 = \frac{I(\sigma^-)-I(\sigma^+)}{I(\sigma^-)+I(\sigma^+)} = \frac{-\begin{Bmatrix} 1 & 1 & 1 \\ J & J & J_f \end{Bmatrix} \sqrt{\tfrac{3}{2}} \mathrm{Im} \langle t^{\dagger}_{11} \rangle}{\dfrac{2(-1)^{J+J_f}}{3\sqrt{2J+1}} + \sqrt{\tfrac{1}{6}} G^I_2 \begin{Bmatrix} 1 & 1 & 2 \\ J & J & J_f \end{Bmatrix} \langle t^{\dagger}_{20} \rangle}, \tag{3}$$

where J is the excited-state angular momentum, J_f is the optical transition's final-state angular momentum, and the $G^I_K(J)$ are factors that determine depolarization due to hyperfine nuclear interactions. The photon intensity $I(\Theta)$ is for light transmitted through a perfect linear polarizer with its pass axis aligned at an angle Θ with respect to the incident beam, while $I(\sigma^+)$ and $I(\sigma^-)$ are the intensities of light with positive and negative helicity along the optical axis of the detector [22]. The terms $\langle t^{\dagger}_{KQ} \rangle = \langle \mathcal{T}^{\dagger}_{KQ} \rangle / \langle \mathcal{T}^{\dagger}_{00} \rangle$ are the ''relative integrated-state multipoles.'' Because of the spin dependence of these multipoles both P_2 and P_3 are proportional to the transverse spin, while P_1 is independent of spin [21].

II. NUMERICAL METHOD

The calculations reported here were performed along the lines described earlier by Zeman and co-workers [5,23,24]. Briefly, the N-electron target states Φ_i were represented as multi-configuration expansions

$$\Phi_i(\mathbf{r}_1, \ldots, \mathbf{r}_N) = \sum_k c_{ik} \phi_k(\mathbf{r}_1 \ldots \mathbf{r}_N). \tag{4}$$

The expansion coefficients and the approximate target energies E^N_i were obtained by diagonalizing the target Hamiltonian H^N according to

$$\langle \Phi_i | H^N | \Phi_j \rangle = E^N_i \delta_{ij}. \tag{5}$$

The configurations ϕ_k were constructed from a bound orbital basis consisting of self-consistent-field (SCF) orbitals whose radial components, $P_{nl}(r)$, were obtained using the CIV3 atomic structure package of Hibbert [25] with the nonrelativistic Hamiltonian H^N used in the optimization procedure. After the orbitals were obtained, the approximate Breit-Pauli Hamiltonian

$$H^N_{\mathrm{BP}} = H^N + H^N_{\mathrm{mass}} + H^N_D + H^N_{\mathrm{SO}}, \tag{6}$$

consisting of the nonrelativistic Hamiltonian and the one-electron relativistic mass correction, Darwin, and spin-orbit terms, was used in the description of the target states.

The input for starting the optimization procedure consisted of the Hartree-Fock orbitals for the respective ground states, as given in the tables of Clementi and Roetti [26]. Further valence orbitals were then constructed for the $4p^5 5s$ and $4p^5 5p$ states, with simultaneous reoptimization of the $4p$ orbital in the ground-state configuration. The reoptimization ensured that this orbital was also a reasonable approximation for use in the excited states of interest. In addition, a $4d$ and a $6s$ valence orbital were constructed to account for the most important channel coupling effects for all the states of interest.

The results presented below were obtained in a 31-state close-coupling approximation, including all states with the configurations $4p^6$, $4p^5 5s$, $4p^5 5p$, $4p^5 4d$, and $4p^5 6s$. The calculated energy level splittings of the states compared very well with experimentally determined values [27], but in order to correct as much as possible for the missing details in the structure calculation, we adjusted the diagonal terms of the Hamiltonian matrix by the very small amounts necessary to obtain the experimental thresholds for the channels coupled to the target states of interest.

The collision calculation was performed using the R-matrix (close-coupling) method that is based upon the partitioning of configuration space into two regions whose boundaries intersect at a specified radial distance $r=a$. In the internal region ($r \leqslant a$) electron exchange and correlation between the scattered electron and the N-electron target are considered important, and the $(N+1)$-electron system is treated as a closed system similar to an atomic structure problem. In the external region ($r > a$) exchange between the scattered electron and the target can be neglected, and hence the calculation is simplified dramatically.

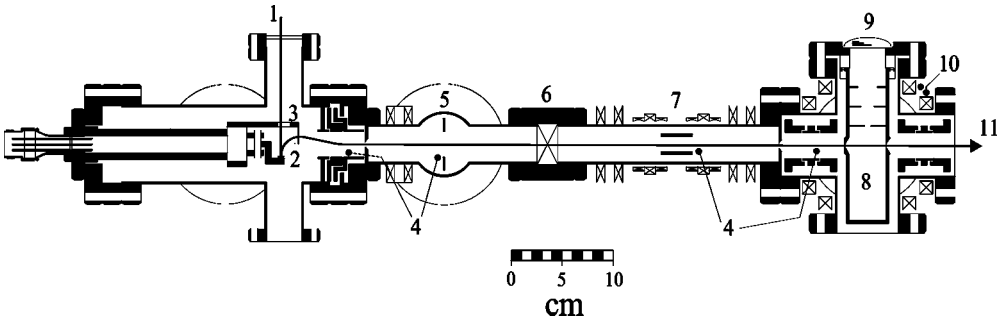

FIG. 1. Diagram of the apparatus showing laser beam (1) for producing photoemitted electrons from the GaAs crystal (2); cylindrical electrostatic bender (3); electrostatic focusing elements (4); differential pumping chamber (5); isolation gate valve (6); solenoidal spin rotators (7); gas target cell (8); fluorescence collection lens and vacuum wall (9); magnetic dipole steering elements (10); electron beam (11).

The Breit-Pauli *R*-matrix code of Berrington, Eissner, and Norrington [28] was used to perform the inner-region calculation. Accounting for partial waves up to a total (target plus projectile) electronic angular momentum of $J_{\mathrm{tot}}=9/2$, with 25 continuum orbitals for each orbital angular momentum of the projectile, ensured converged results for energies up to about 5 eV above the thresholds of interest. The calculation for the external region was performed using the flexible asymptotic *R*-matrix (FARM) package by Burke and Noble [29]. For each collision energy, this yields the reactance (**K**), scattering (**S**), and transition (**T**) matrices from which the Stokes parameters of interest were calculated following the procedure outlined by Bartschat *et al.* [30].

III. EXPERIMENTAL METHOD

For the measurements reported here, we investigated excitation of the well *LS*-coupled $4p^5 5p[5/2]\ {}^3D_3$ and the intermediately coupled $4p^5 5p[5/2]\ {}^3D_2$ states of Kr with polarized electrons having energies up to 1.2 eV above the respective excitation thresholds of these states. The threshold of the first state which can cascade into the ${}^3D_3$ level is 12.11 eV. Likewise, the threshold of the first level which can cascade into the ${}^3D_2$ level is 12.03 eV. Thus, there are 0.7 eV and 0.6 eV ''windows'' of cascade-free fluorescence above each respective excitation threshold.

As a source of polarized electrons (Fig. 1), we used the (100) face of bulk *p*-type Zn-doped GaAs [31,32]. We produced a longitudinally polarized electron beam by photoemission from the GaAs using a circularly polarized GaAlAs diode laser at 780 nm (Lasiris model DLS-500-780-50). To obtain efficient photoemission, we activated the crystal to negative electron affinity using the yo-yo technique described by Tang *et al.* [33]. The longitudinal polarization of the beam was transformed into transverse polarization by bending the beam 90° with a unique electrostatic deflector, which rotated its momentum without affecting its spin. We have observed emission currents of 40 μA with 40 mW of laser power and electron polarizations of 0.28(3). A more detailed description of this polarized electron source can be found in Ref. [32].

The electron beam was transported down the beamline using electrostatic lenses and magnetic steering coils (see Fig. 1). The beam also passed through a soleniodal spin rotator which could correct for any spurious rotation of the electron spin. After being transported 50 cm the electron beam entered a stainless steel target cell through a 1 mm diameter beam-defining aperture, excited the target gas, exited through a 2.0 mm diameter aperture, and was detected on a series of downstream lens elements.

Our target cell was constructed of a stainless steel can. The top of the cell was isolated from the chamber by a gastight connection to a ring of Macor and was capped by a Viton seal to the photon collection lens. Target gas was delivered to the cell through a stainless steel tube which passed through the outer wall of the cell. The pressure was controlled by a Granville Phillips 203 leak valve. A pressure buffer composed of a wad of crumpled and sooted copper mesh was placed over the gas entrance at the bottom of the cell.

The resonance fluorescence produced in the vertical direction (along the electron spin axis) was focused into a parallel beam by the photon collection lens (51 mm diameter, 101 mm focal length) at the top of the gas cell. These photons then passed through an optical polarimeter composed of a linear polarizer / quarter-wave plate combination similar to that described by Berry *et al.* [34]. The photons were then counted by a GaAs photomultiplier tube (Hamamatsu model R943-02).

Since we knew that the linear polarization fraction P_2 is quite small [Furst *et al.* [8,9] measured it to be $4(4)\times10^{-3}$ at 0.7 eV above threshold], we had to design our apparatus and experimental procedure to reduce statistical uncertainty and eliminate spurious systematic effects. The target cell was carefully designed to measure the relative Stokes parameters near threshold precisely. We chose to use a static gas cell in the present experiments rather than the effusive beam target of Furst *et al.* to increase the target density-length product from $\sim5\times10^{10}$ cm^{-2} to $\sim5\times10^{12}$ cm^{-2}. Because of the Kr pressures in the target cell, it was necessary to add a differential pumping stage to the beam line so that the pressure in the source region would not diminish the GaAs quantum efficiency. We were able to increase the pressure ratio between the target cell and the source chamber to $\sim10^4$ by using a 55 l/s turbo pump and two 5 mm apertures at the entrance and exit of the differential pumping chamber. The higher target density resulted in a significantly higher count rate and an accompanying improvement in the statistical precision of our data.

Precautions were taken to accurately determine signal rate very near threshold where the background rate is a large portion of the total count rate. First, we cooled the photomul-

tiplier tube to $-26\,^{\circ}\mathrm{C}$, which reduced the dark count rate to ≈ 10 Hz. Next, we made several efforts to reduce the background due to stray photons. The entire target cell, including the copper mesh pressure buffer, was heavily sooted using an acetylene torch. The mesh absorbed photons from the interaction region that were emitted directly away from the photon collection lens. Furthermore, a series of light apertures were used to define the visible interaction volume and absorb reflected photons. Along with the electron beam entrance and exit apertures, these light apertures limited the visible interaction volume to a cylinder 8 mm long and 1.5 mm in diameter. Additionally, we improved our estimate of the background count rate by measuring the background at several energies below threshold for each excitation function. Finally, we minimized the problems associated with drifting experimental parameters by taking the data quickly using a computer to control the electron energy accurately and repeatably. Each data set was composed of several excitation functions, one for each combination of linear polarizer position and electron polarization. The data were analyzed in several steps. First, the dark counts were removed. Then, the data were normalized to pressure and current to remove the effects of drifting experimental parameters. Finally, the residual background was removed and the modified excitation functions were combined and analyzed to yield polarization measurements as a function of energy.

Carefully accounting for the background in this way allowed us to obtain data consistent with the kinematically required threshold value of P_1 (0.41) for the $^3D_3$ state. In this regard, we note that the threshold is defined as being one-half step (0.05 eV) below the energy at which the signal rate becomes statistically distinct from the background. This convention has the advantage that the lowest-energy polarizations should be consistent with the kinematic threshold values, regardless of the energy distribution of the electron beam. Furthermore, graphs of the measured polarizations begin at the actual energy threshold and can be compared directly to any theoretical calculation, after appropriate electron beam energy profile convolutions have been made (see below).

Additionally, we carefully examined our apparatus for possible systematic errors and eliminated them. We corrected for the small relative reduction ($\leqslant 1.3\%$) in the Stokes parameters due to the finite collision volume, slightly divergent electron beam (3.5° half angle), and finite photon aperture (11° half angle) [35]. Additionally, we used magnetic coils outside the vacuum chamber to cancel stray magnetic fields in the target region, which could have altered the fluorescence radiation through the Hanle effect [20]. Figure 2 demonstrates the effect of a magnetic field on the linear polarization fractions P_1 and P_2 when the field vectors, electron spin, and photon emission are all along the same axis. For the data presented here, the $^3D_3$ state was excited with unpolarized electrons which would produce pure P_1 polarization in the absence of a magnetic field. The nonzero values of P_2 in Fig. 2 were produced when the plane of polarization was rotated due to the precession of the excited states in the magnetic field. It is clear that large magnetic fields destroy both P_1 and P_2, and that even small magnetic fields can produce spurious results. These results emphasize the necessity of carefully eliminating magnetic fields for accurate Stokes parameter measurements.

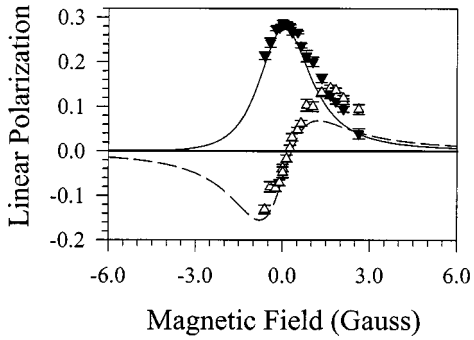

FIG. 2. Integrated Stokes parameters P_1 and induced P_2 as a function of magnetic field in the target region for the 811 nm transition excited by unpolarized electrons at 12.4 eV (see text). The data are represented by triangles, and theoretical Hanle effect values by lines. The magnetic-field measurement is accurate to 20%. (P_1 solid triangles and solid line; P_2, open triangles and dashed line.)

We averaged four measurements of P_1 and P_2 at the four equivalent pairs of linear polarizer angles to eliminate rotational optical asymmetries. We also made each measurement of the spin-dependent parameters P_2 and P_3 with the spin polarization of the incident electron beam both parallel and antiparallel to the optical axis of the polarimeter. This optical spin reversal technique is particularly effective in eliminating spin-independent instrumental asymmetries and effects due to possible spurious magnetic fields in the interaction volume.

We investigated the dependence of the measured polarization on target pressure (Fig. 3), and found that depolarization became significant at pressures above 4×10^{-4} Torr. This is consistent with the results of Chilton *et al.* [36]. All of the results reported here were obtained with target pressures below 1.5×10^{-4} Torr. It is probable that there is no significant pressure dependence of the Stokes parameters below 3×10^{-4} Torr. But even in a worst case, for polarization rising linearly to zero pressure, measurements made at 1.5×10^{-4} Torr would be systematically low by only about 0.3% for the situation illustrated in Fig. 3, or about 1.3% of the quoted value. Such errors are not significant given the scatter and statistical uncertainty of our data.

We also investigated the energy width (ΔE) of the pho-

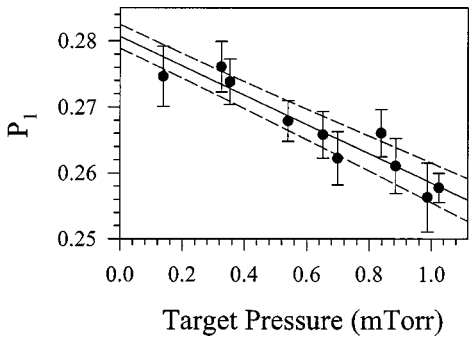

FIG. 3. Depolarization of 811 nm resonance fluorescence vs target pressure at 12.4 eV. The solid line represents an error-weighted least-squares fit to the data. The dotted lines represent the uncertainty in the fit. Pressure is accurate to 25%.

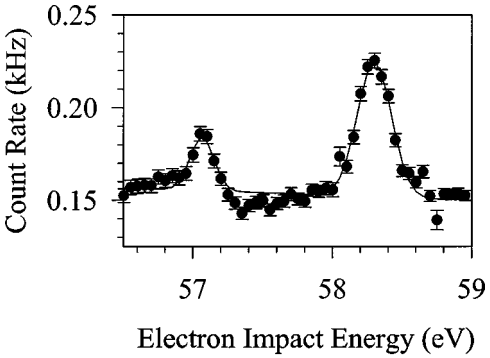

FIG. 4. Optical intensity of the He $3\,^3D \rightarrow 2\,^3P$ transition excited by electron impact. The resonance features are due to cascades from the $2s^2 2p\,^2P$ and $2s2p^2\,^2D$ negative-ion resonances at 57.15 eV and 58.23 eV, respectively. The natural linewidth of the ^2D resonance is $\Gamma = 0.025 \pm 0.010$ eV [39], which implies that the FWHM of the present electron beam is approximately 0.3 eV. The solid line represents two Gaussians plus background fit to data.

toemitted electron beam. Knowledge of this width is crucial in this experiment, where we are comparing measurements with theoretical results having features as narrow as 0.1 eV. Furthermore, reports in the literature have indicated that ΔE can grow with both larger emission current [37] and higher GaAs temperature [38]. We determined our beam's ΔE by scanning its energy across the narrow ($\leqslant 25$ meV) $2s2p^2\,^2D$ negative-ion resonance in He [39] and observing the subsequent $3\,^3D \rightarrow 2\,^3P$ fluorescence. A typical data set is plotted in Fig. 4. Because of the narrow resonance width, the beam energy width is essentially given by the width of the fluorescence peak. Using this technique, we determined ΔE [full width at half maximum (FWHM)] to be 0.3(.05) eV for the operating conditions of our source. Unlike Ref. [37] we found no statistically significant variation of ΔE with extracted beam current over the range in which we operated ($\leqslant 10\ \mu$A).

IV. RESULTS

In this section, we compare the measured integrated Stokes parameters for the 811 nm transition from the well LS-coupled $^3D_3$ state and the 878 nm transition from the intermediately coupled $^3D_2$ state to those predicted by the 31-state R-matrix calculation. To compare these results directly, we needed to account for the effect of the finite electron beam energy width ΔE on the calculated polarizations. Since we observed the fluorescence through polarization optics, the convolution of the calculation with the electron beam profile must be performed on the individual polarization components before they are combined to yield the Stokes parameters. We assumed an electron beam profile of a Gaussian with an asymmetric low-energy tail, similar to the profiles observed by Kolac *et al.* [37].

We discuss the integrated Stokes parameters of the 811 nm transition first. Figure 5 is comprised of our present data, the data of Furst *et al.* [9], and our calculation. The three sets of data for the linear polarization fraction P_1 agree qualitatively (notice that the figure has a suppressed zero). The gross features of the present experimental data also compare well with the R-matrix calculation, i.e., the present data have

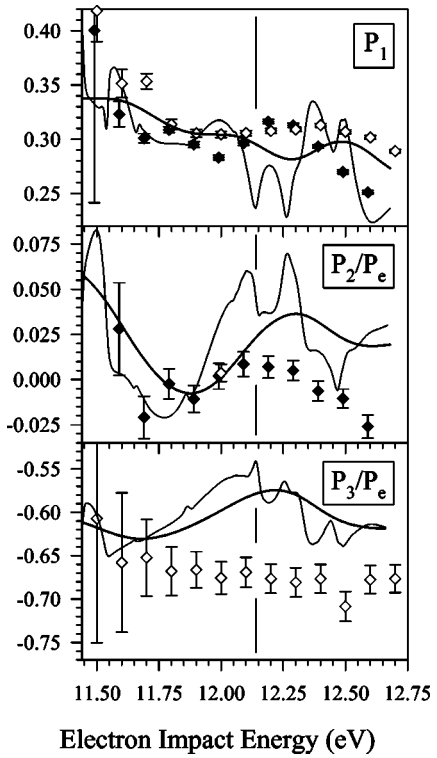

FIG. 5. Integrated Stokes parameters for the 811 nm transition in Kr $(4p^5 5p[5/2]\,^3D_3 \rightarrow 4p^5 5s[3/2]\,^3P_2)$. The solid diamonds are the present data. The open diamonds are the data of Furst *et al.* [9]. The thin line is the R-matrix calculation, while the thick line is the calculation convoluted with a 0.3 eV FWHM asymmetric Gaussian profile (see text). The vertical line at 12.14 eV represents the cascade threshold.

the same configuration of bumps and dips. However, the bump at 12.25 eV in the present data is more pronounced than that of Furst *et al.* There also seems to be an energy shift among the results, which might explain why the polarization of the present data begins to fall at a lower energy than that of Furst *et al.*, and why there seems to be a misalignment with the convoluted theoretical curve. More importantly, though, there are places where the two experimental data sets disagree by several standard deviations. We can offer no explanation for this, but must attribute it to the significant differences between the two apparatuses we used.

The present P_2 data are consistent with the datum of Furst *et al.* For energies below 12.11 eV, the first cascading threshold for the $^3D_3$ state, our data are consistent both with zero and the convoluted theory. Only above 12.3 eV do the data deviate significantly from zero. However, this may be the result of cascading (only one of the lowest-lying cascading levels is a Russell-Saunders state). Assuming the theory is correct, it should be possible to measure a nonzero value of P_2 at about 11.6 eV. However, this is a very difficult measurement because the polarization is small and the background and signal rates are roughly equal. The P_3 data of Furst *et al.* (Fig. 5), like the present data for P_1 and P_2, are qualitatively similar to the convoluted theory curve (note again the suppressed zero).

The integrated Stokes parameters of the 878 nm transition in Kr $(4p^5 5p[5/2]\,^3D_2 \rightarrow 4p^5 5s[3/2]\,^3P_1)$ are presented in Fig. 6. Here, the agreement between the measured results and

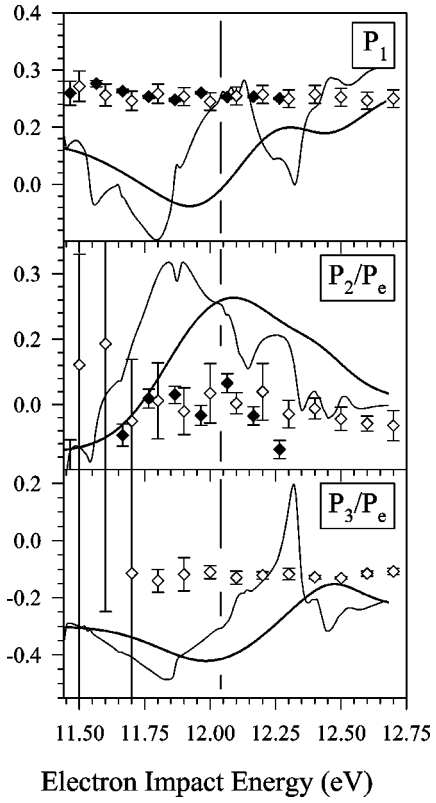

FIG. 6. Integrated Stokes parameters for the 878 nm transition in Kr ($4p^5 5p[5/2]\,^3D_2 \rightarrow 4p^5 5s[3/2]\,^3P_1$). The vertical line at 12.04 eV represents the cascade threshold. All other designations are as in Fig. 5.

the theory is generally abysmal. For P_1, P_2, and P_3 the measured data are consistent with each other over their entire common range. There is no evidence for the broad energy-dependent features predicted by the theory. Indeed, neither experimental data set has any significant energy dependence for any of the integrated Stokes parameters.

All of this, taken together, indicates that the relative Stokes parameters predicted by the present *R*-matrix calculation are much more reliable for the 811 nm transition from the well *LS*-coupled $^3D_3$ state than for the 878 nm transition from the intermediately coupled $^3D_2$ state. This may be explained solely by problems in the structure calculation for the intermediately coupled $4p^5 5p\,^3D_2$ state.

V. CONCLUSIONS

For the case of electron-impact excitation of the well *LS*-coupled $4p^5 5p\,^3D_3$ state in Kr, the Breit-Pauli *R*-matrix approach does a good, qualitative job of describing the integrated Stokes parameters P_1, P_2, and P_3, with the caveat that cascading, which is not accounted for in the theory, is responsible for the discrepancies above 12.1 eV incident energy. For the intermediately coupled $4p^5 5p\,^3D_2$ state, none of the integrated Stokes parameters are predicted satisfactorily. It is thus evident that the present theoretical description, although being the state-of-the-art method for treating these collisions, needs to be improved. This could be achieved by a relatively straightforward (though computationally very challenging) extension of the *R* matrix with pseudostate (RMPS) method, described by Bartschat *et al.* [40], to include relativistic effects. In such calculations, the description of both the collision process and the target structure would likely be improved. On the other hand, it is also clear that experimentalists must possess good knowledge of the characteristics of their apparatuses in order to allow for meaningful comparisons between experiment and theory at a detailed level.

ACKNOWLEDGMENTS

This work was supported by NSF Grant Nos. PHY-973520 (Nebraska) and PHY-9605124 (V.Z. and K.B.).

[1] I. Bray and A.T. Stelbovics, Adv. At., Mol., Opt. Phys. **35**, 209 (1995).
[2] D.V. Fursa, I. Bray, B.P. Donnelly, D.T. McLaughlan, and A. Crowe, Phys. Rev. A **56**, 4606 (1997).
[3] K.A. Berrington, W.B. Eissner, and P.H. Norrington, Comput. Phys. Commun. **92**, 290 (1995).
[4] V. Zeman and K. Bartschat, J. Phys. B **30**, 757 (1997).
[5] V. Zeman, K. Bartschat, T.J. Gay, and K.W. Trantham, Phys. Rev. Lett. **79**, 1825 (1997).
[6] N.S. Scott and K.T. Taylor, Comput. Phys. Commun. **25**, 347 (1982).
[7] K. Bartschat and K. Blum, Z. Phys. A **304**, 95 (1982).
[8] J.E. Furst, T.J. Gay, W.M.K.P. Wijayaratna, K. Bartschat, H. Geesmann, M.A. Khakoo, and D.H. Madison, J. Phys. B **25**, 1089 (1992).
[9] J.E. Furst, W.M.K.P. Wijayaratna, D.H. Madison, and T.J Gay, Phys. Rev. A **47**, 3775 (1993).
[10] R. Srivastava, R.P. McEachran, and A.D. Stauffer, J. Phys. B **28**, 869 (1995).
[11] D.H. Yu, P.A. Hayes, J.E. Furst, and J.F. Williams, Phys. Rev. Lett. **78**, 2724 (1997).
[12] P.A. Hayes, D.H. Yu, J. Furst, M. Donath, and J.F. Williams, J. Phys. B **29**, 3989 (1996).
[13] M. Uhrig, G.F. Hanne, and J. Kessler, J. Phys. B **27**, 4009 (1994).
[14] M. Uhrig, S. Hörnermann, M. Klose, K. Becker, and G.F. Hanne, Meas. Sci. Technol. **5**, 1239 (1994).
[15] D.H. Yu, P.A. Hayes, J.F. Williams, and C. Locke, J. Phys. B **30**, L461 (1997).
[16] D.H. Yu, P.A. Hayes, and J.F. Williams, J. Phys. B **30**, L487 (1997).
[17] R. Srivastava, K. Blum, R.P. McEachran, and A.D. Stauffer, J. Phys. B **29**, 5947 (1996).
[18] R.E.H. Clark, G. Csanak, and J. Abdallah, Jr., Bull. Am. Phys. Soc. **43**, 1273 (1998).
[19] T.J. Gay, J.E. Furst, K.W. Trantham, and W.M.K.P. Wijayaratna, Phys. Rev. A **53**, 1623 (1996).
[20] K. Blum, *Density Matrix Theory and Applications*, 2nd ed. (Plenum, New York, 1996).

[21] K. Bartschat, K. Blum, G.F. Hanne, and J. Kessler, J. Phys. B **14**, 3761 (1981).
[22] D.H. Yu, P.A. Hayes, J.F. Williams, and J.E. Furst, J. Phys. B **30**, 1799 (1997).
[23] V. Zeman and K. Bartschat, J. Phys. B **30**, 4609 (1997).
[24] V. Zeman, K. Bartschat, C. Norén, and J.W. McConkey, Phys. Rev. A **58**, 1275 (1998).
[25] A. Hibbert, Comput. Phys. Commun. **9**, 141 (1975).
[26] E. Clementi and C. Roetti, At. Data Nucl. Data Tables **14**, 177 (1974).
[27] C.E. Moore, *Atomic Energy Levels*, Natl. Bur. Stand. (U.S.) No. NSRDS-NBS 35 (U.S. GPO, Washington, DC, 1971).
[28] K.A. Berrington, W.B. Eissner, and P.H. Norrington, Comput. Phys. Commun. **92**, 290 (1995).
[29] V.M. Burke and C.J. Noble, Comput. Phys. Commun. **85**, 471 (1995).
[30] K. Bartschat, N.S. Scott, K. Blum, and P.G. Burke, J. Phys. B **17**, 269 (1984).
[31] D.T. Pierce, R.J. Celotta, G.C. Wang, W.N. Unertl, A. Galejs, C.E. Kuyatt, and S.R. Mielczarek, Rev. Sci. Instrum. **51**, 478 (1980).
[32] H.M. Al-Khateeb, B.G. Birdsey, T.C. Bowen, A.S. Green, M.E. Johnston, and T.J. Gay (unpublished).
[33] F.C. Tang, M.S. Lubell, K. Rubin, A. Vasilakis, M. Eminyan, and J. Slevin, Rev. Sci. Instrum. **57**, 3004 (1986).
[34] H.G. Berry, G. Gabrielse, and A.E. Livingston, Appl. Opt. **16**, 3200 (1977).
[35] V.J. Ehlers and A.C. Gallagher, Phys. Rev. A **7**, 1573 (1972).
[36] J.E. Chilton, J.B. Boffard, R.S. Schappe, and C.C. Lin (private communication).
[37] U. Kolac, M. Donath, K. Ertl, H. Liebl, and V. Dose, Rev. Sci. Instrum. **59**, 1933 (1988).
[38] C.S. Feigerle, D.T. Pierce, A. Seiler, and R.J. Celotta, Appl. Phys. Lett. **44**, 866 (1984).
[39] J.J. Quèmèner, C. Paquet, and P. Marmet, Phys. Rev. A **4**, 494 (1971).
[40] K. Bartschat, E.T. Hudson, M.P. Scott, P.G. Burke, and V.M. Burke, J. Phys. B **29**, 115 (1996).